

# The 2004 Hyperflare from SGR 1806-20: Further Evidence for Global Torsional Vibrations

Tod E. Strohmayer<sup>1</sup> and Anna L. Watts<sup>2</sup>

## ABSTRACT

We report an analysis of the archival Rossi X-ray Timing Explorer (RXTE) data from the December 2004 hyperflare from SGR 1806-20. In addition to the  $\approx 90$  Hz QPO first discovered by Israel et al., we report the detection of higher frequency oscillations at  $\approx 150$ , 625, and 1,840 Hz. In addition, we also find indications of oscillations at  $\approx 720$ , and 2,384 Hz, but with lower significances. The 150 Hz QPO has a width (FWHM) of about 17 Hz, an average amplitude (rms) of 6.8%, and is detected in average power spectra centered on the rotational phase of the strongest peak in the pulse profile. This is approximately half a cycle from the phase at which the 90 Hz QPO is detected. The 625 Hz oscillation was detected in an average power spectrum from nine successive cycles beginning approximately 180 s after the initial hard spike. It has a width (FWHM) of  $\approx 2$  Hz and an average amplitude (rms) during this interval of 8.5%. We find a strong detection of the 625 Hz oscillation in a pair of successive rotation cycles beginning about 230 s after the start of the flare. In these cycles we also detect the 1,840 Hz QPO. When the 625 Hz QPO is detected we also confirm the simultaneous presence of 30 and 92 Hz QPOs. The centroid frequency of the 625 Hz QPO detected with RXTE is within 1 Hz of the  $\approx 626$  Hz oscillation recently found in RHESSI data from this hyperflare by Watts & Strohmayer. We argue that these new findings provide further evidence for a connection of these oscillations with global oscillation modes of neutron stars, in particular, the high frequency signals may represent toroidal modes with at least one radial node in the crust. We discuss their implications in the context of this model, in particular for the depth of neutron star crusts.

*Subject headings:* stars: magnetic—pulsar: individual (SGR 1806-20)—stars: neutron—stars: rotation—stars: oscillations—X-rays: stars

---

<sup>1</sup>Exploration of the Universe Div., NASA/GSFC, Greenbelt, MD 20771; stroh@milkyway.gsfc.nasa.gov

<sup>2</sup>Max Planck Institut für Astrophysik, Karl-Schwarzschild-Str. 1, 85741 Garching, Germany; anna@mpa-garching.mpg.de

## 1. Introduction

Recent studies of high time resolution data from two magnetar hyperflares recorded by the Proportional Counter Array (PCA) onboard the Rossi X-ray Timing Explorer (RXTE) have resulted in the discovery of a new phenomenon associated with these events. Both the December, 2004 event from SGR 1806-20, and the August, 1998 hyperflare from SGR 1900+14 produced fast, rotation-phase-dependent X-ray oscillations in the 20 - 150 Hz range. First, Israel et al. (2005) reported the discovery of  $\approx 18, 30,$  and 90 Hz quasi-periodic oscillations (QPO) in the December, 2004 event, and suggested that the 30 and 90 Hz QPOs could be linked with seismic vibrations of the neutron star crust. Strohmayer & Watts (2005) then reported the discovery of a sequence of QPOs in the SGR 1900+14 hyperflare. They found a set of frequencies; 28, 53.5, 84, and 155 Hz, which could plausibly be associated with a sequence of low  $l$  toroidal modes (denoted  ${}_l t_0$ ) of the elastic neutron star crust (see, for example, Hansen & Cioffi 1980; McDermott, van Horn & Hansen 1988; Duncan 1998; Piro 2005). In both hyperflares the oscillations are episodic, that is, their amplitudes vary considerably with time and rotational phase. Most recently, Watts & Strohmayer (2006) examined Ramaty High Energy Solar Spectroscopic Imager (RHESSI) data for the SGR 1806-20 event, confirmed the presence of the 18 Hz and 90 Hz QPOs, and found evidence for additional oscillations at 26 Hz and 626 Hz.

The similar phenomenology of the oscillations in the two sources, as well as the closeness of some of the measured frequencies argues rather convincingly that we are seeing the same physical process in each case. The connection with torsional modes of the crust seems plausible for several reasons; 1) The observed frequencies are consistent with theoretical expectations for such modes, and can be more or less self-consistently associated with a sequence of modes with varying spherical harmonic index,  $l$ . 2) The magnetic instability which powers the hyperflares is likely associated with large scale fracturing of the neutron star crust (Flowers & Ruderman 1977; Thompson & Duncan 1995; Duncan 1998; Thompson & Duncan 2001; Schwartz et al. 2005), and will almost certainly generate seismic motions within the star. 3) The strong phase dependence argues for a mechanism associated with particular sites on the stellar surface, such as a fracture zone or magnetic field bundle. 4) Mechanical motions provide a natural explanation for the relatively high coherence of the oscillations. 5) Horizontal motions of the crust could modulate the beaming pattern associated with the strong magnetic field, providing a mechanism to modulate the X-ray flux. Moreover, beaming can act as an “amplifier,” producing potentially large X-ray modulations from modest horizontal displacements. Although the present evidence for torsional modes is very suggestive, it is not yet definitive. Levin (2006), for example, argues that toroidal modes may damp too quickly to account for the detection of oscillations some minutes after the onset of the flare. In addition some of the detected frequencies (18 Hz, 26 Hz) do not

fit easily into current torsional mode models, without invoking magnetic splitting or other complications.

In our previous study of the RXTE data from the SGR 1900+14 hyperflare we computed average power spectra for different rotational phases and time intervals during the event. This method should be more sensitive to oscillations which are localized in rotational phase, as borne out in the SGR 1900+14 study. In this paper we report the results of a similar, phase averaged timing study on the now public archival RXTE data from the SGR 1806-20 hyperflare. Using this method we find strong evidence for additional, higher frequency oscillations during the flare.

## 2. Observations and Data Analysis

An overview of the RXTE data recorded from the December, 2004 hyperflare from SGR 1806-20 is given by Israel et al. (2005). Data were recorded in the “Goodxenon\_2s” mode that allows for time resolution up to  $\approx 1 \mu\text{s}$ . The hyperflare intensity profile, folded at the rotational frequency (see Figure 1), shows 3 peaks. In subsequent discussions we will refer to these as peaks 1, 2, and 3, in order of decreasing peak intensity, respectively. We will also refer to the region of pulse phase between peaks 2 and 3 as the “interpulse” region.

### 2.1. KiloHertz Oscillations

Since previous studies have shown the  $\approx 90$  Hz QPO to be extremely robust, and its approximate location in rotational phase has been linked to the interpulse region, by both Israel et al. (2005) and Watts & Strohmayer (2006), we began our study by computing average power spectra around this phase range, but for a sequence of different time intervals during the flare. We used 3 s intervals to compute each individual power spectrum and we initially restricted our search to a Nyquist frequency of 4096 Hz, although these PCA data can, in principle, be used to sample to much higher frequencies. We found a significant signal at 625 Hz in power spectra computed from approximately the last third of the hyperflare. We now discuss the detection, significance and properties of this oscillation.

Figure 2 shows an average power spectrum computed from 9 successive rotations starting approximately 190 s after the onset of the hyperflare. Both the time interval during the flare (top), and the phase region (bottom, dashed lines) used in computing this spectrum are shown in Figure 1. This power spectrum has a prominent feature at 625 Hz, and the QPO at 92 Hz is also clearly detected. To estimate the significance of the 625 Hz feature we extended

the frequency range to 65 kHz, and used all frequency bins above 800 Hz to estimate the noise power distribution. Figure 2 shows the power spectrum to 65 kHz (main panel), as well as the distribution of noise powers (inset panel). We fit the noise power histogram with a  $\chi^2$  function, and found a reasonable fit for 87 degrees of freedom (dof), and a small reduction in the Poisson level of 0.01. This function is also plotted in the inset panel of Figure 2 (solid curve). Using this noise distribution we find a single trial significance of  $7 \times 10^{-11}$  for the 625 Hz feature. The power spectrum has 1,536 bins up to 4096 Hz (2.66 Hz resolution), which was the top end of our search range. We emphasize that we extended the frequency range only *after* the search, simply to better characterize the noise power distribution. This gives a probability of  $1.1 \times 10^{-7}$  to find a peak this high in the power spectrum. The spectrum shown in Figure 2 was one of a sequence from across the entire duration of the flare. We computed these by overlapping the time intervals, so each spectrum in the sequence is not fully independent. However, even using the total number of spectra computed (47), we have a significance  $< 1 \times 10^{-5}$ , so this is a robust detection. We fit the QPO with a Lorentzian profile and find a center frequency and width of  $625.5 \pm 0.15$  Hz, and  $1.8 \pm 0.4$  Hz, respectively. The 625 Hz QPO has an average amplitude during this interval of 8.5%. We further note that the strength of the 625 Hz feature is comparable to that of the 92 Hz signal, which provides additional confidence that it is not simply a statistical fluctuation.

We searched the RHESSI data to see if there was any indication of a simultaneous 625 Hz peak but did not detect anything significant at this time. This is however not surprising given the amplitude, and the fact that for such high frequencies we can only use the RHESSI front segments, which have a much lower countrate than RXTE (see the discussion in Watts & Strohmayer (2006)). In addition the RXTE signal is strongest at energies less than 45 keV; at low energies the RHESSI spectrum exhibits much higher background levels, which could swamp such a weak signal.

We computed dynamic power spectra in the vicinity of 625 Hz to search for time dependence of the signal. The results suggest that the 625 Hz oscillation is most strongly associated with the falling edge of peak 2 of the pulse profile, and that its amplitude can vary strongly with time. For example, Figure 3 shows a portion of the hyperflare that contributes strongly to the 625 Hz signal detected in the average power spectrum described above. Contours of constant Fourier power in the vicinity of 625 Hz are plotted over the hyperflare profile. We used 1/2 s intervals and started a new interval every 0.1 s. One pulsation cycle is plotted. The strong correlation of power contours with the falling edge of peak 2 is rather similar to the behavior seen in the 84 Hz oscillation from SGR 1900+14 (Strohmayer & Watts 2005, see their Figure 3), and these similarities suggest it may be connected with the X-ray modulation mechanism.

We also computed several average power spectra in the immediate temporal vicinity of the strong 625 Hz signal seen in the dynamic power spectrum. An average from two consecutive rotation cycles beginning with the cycle prior to that shown in Figure 3 reveals evidence for an oscillation at an even higher frequency of 1,840 Hz. The average power spectrum from these two cycles is shown in Figure 4. The two spectra are the same except for being plotted at different resolutions. We reiterate that the phase range used here (and for Figure 5 below) is the same as for Figure 2 (denoted by the vertical dashed lines in Figure 1). The peak at 1,840 Hz is most prominent in the top trace, at 5.33 Hz resolution (the bottom trace has 2.66 Hz resolution). Both the 92 Hz and 625 Hz peaks also stand out prominently in this spectrum. We estimated the significance in the manner discussed above, and found chance probabilities of  $1.1 \times 10^{-6}$ , and  $1.1 \times 10^{-5}$  for the 625 and 1,840 Hz peaks, respectively. This is an estimate of the probability of finding a peak as high as those observed in this power spectrum up to 4096 Hz. We computed eight such spectra, so this will reduce the significances somewhat, but again, the detections are further supported by the comparable amplitude of these peaks to that of the well established 92 Hz oscillation, which is also detected in the same power spectrum. The average amplitudes for the 625 and 1,840 Hz oscillations over these two cycles are 18.3 and 18.0 % (rms) respectively.

We also see weaker indications for a few additional high frequency peaks during this time interval. Figure 5 compares two power spectra, one (top) from the two cycle interval in which the 1,840 Hz signal is seen, and the other (bottom) an average of two cycles beginning six cycles earlier than the cycle shown in Figure 3. The frequency resolution is 10.66 Hz in both plots. The top spectrum is actually the same as in Figure 4, but plotted with lower resolution. The 625 and 1,840 Hz peaks still stand out prominently. We estimated the standard deviation in the noise distribution as before, and we placed two horizontal dotted lines  $4\sigma$  (single trial) above the mean in each case. In the bottom spectrum, there are also two peaks which reach above the  $4\sigma$  line. These have frequencies of 720 and 2,384 Hz. We estimate significances (single trial) of  $4.4 \times 10^{-6}$  and  $1.3 \times 10^{-5}$ , respectively, for these peaks. A third peak, at 976 Hz, does not reach the  $4\sigma$  line, but is a  $3\sigma$  deviation, with an estimated significance of  $7.6 \times 10^{-4}$ . While we do not claim that all these peaks represent strong detections, it does seem unlikely by chance to have several such sizable deviations from the mean in a single spectrum, and thus we think this could be an indication of the presence of additional, weaker signals in the data.

We also searched the RXTE data for evidence of a 626 Hz QPO earlier in the tail, when a QPO of that frequency was seen in the RHESSI data (Watts & Strohmayer 2006). We were not able to find a corresponding signal in the PCA data. However, this is not entirely surprising. The 626 Hz signal was only observed in the RHESSI data for photons with recorded energies in the range 100-200 keV. Whilst RHESSI is sensitive at these energies,

the PCA does not record photons with energies above  $\approx 100$  keV. Comparing spectra from the two spacecraft is difficult because of the scattering caused by the oblique incidence angles. However we can get some idea of the magnitude of the energy shift between the two datasets by comparing the positions of the spectral maxima. For the PCA the maximum is at 20 keV, for RHESSI it is at 40 keV. If incident photons are downshifted in energy by only 20 keV for the RXTE PCA compared to RHESSI, then we would not expect to see the RHESSI 626 Hz signal, since the PCA does not capture sufficient high energy photons. Unfortunately the RXTE High Energy X-ray Timing Experiment (HEXTE), which covers a higher energy range than the PCA, recorded the main flare but not the decaying tail (Smith et al. 2005).

## 2.2. 150 Hz Oscillation

We also computed average power spectra centered on the rotational phase of peak 1. Figure 1 shows the range of phases used (dashed-dot lines). Average power spectra centered on this phase over the entire hyperflare show a significant QPO centered near 150 Hz. Figure 6 shows the power spectrum in which we detected this QPO. We averaged 45, 3 second power spectra, and the frequency resolution is 8 Hz. The peak near 150 Hz is evident. We modelled the power continuum in the range above 30 Hz with a constant plus a power law, and then rescaled the spectrum by dividing by the best fitting continuum model. We then estimated the noise power distribution in the same way as described earlier, by fitting a  $\chi^2$  distribution to a histogram of noise powers in the rescaled spectrum. Based on this we estimate a significance for the highest bin in the QPO profile as  $2.8 \times 10^{-5}$ , which includes the number of frequency bins searched (up to 4096 Hz). This is a very conservative estimate of the QPO significance, because it only uses the highest bin, and the QPO peak is resolved at this frequency resolution. We fit the QPO profile with a lorentzian and find a centroid frequency of  $150.3 \pm 1.6$  Hz, a width of  $17 \pm 5$  Hz, and an amplitude (rms) of  $6.8 \pm 1.3\%$ . If we construct averages from the first and second halves of the hyperflare, we still detect the 150 QPO, so this oscillation seems to persist through most of the hyperflare. This feature is not detected in the RHESSI data, but this is not unexpected given the low amplitude of the QPO and the lower countrates of the RHESSI front segments.

## 2.3. Lower frequency QPOs

Israel et al. (2005) reported the marginal detection of 18 Hz and 30 Hz QPOs over a period late on in the burst, without exploring for any phase dependence. Watts & Strohmayer (2006) then found evidence in the RHESSI dataset for broad QPOs at 18 and 26 Hz, with

a weaker feature at 30 Hz. These QPOs showed a strong rotational phase dependence, appearing at the same phase as the 92.5 Hz QPO. For these lower frequency QPOs we were able to include photons detected by the RHESSI rear segments, so that the RHESSI countrate exceeded that recorded by RXTE.

The broad QPOs at 18 Hz and 26 Hz were seen in the RHESSI dataset between 60 and 230s after the main flare. We were interested to see whether these QPOs were detectable in the RXTE data. Folding up exactly the same time period and rotational phase used in the RHESSI analysis we were unable to make a statistically significant detection, not unexpected given the discrepancy in countrates and the low fractional amplitude of the QPOs. We therefore focused on two shorter periods in the RHESSI data when the 18 Hz and 26 Hz oscillations were particularly strong, and searched for them at corresponding times in the RXTE data. In both of these cases corresponding peaks are observed in the RXTE data, confirming the detection of QPOs at these frequencies (Figure 7). Interestingly the 26 Hz QPO was stronger in this period in the RXTE dataset than it is in RHESSI, suggesting that other factors may offset the higher countrate (see below).

What about the 30 Hz QPO? If we consider the same time interval indicated in Figure 1, but shift the phase range over which we compute power spectra to later phases, that is, exclude the falling edge of peak 2, the 625 Hz signal drops to undetectable levels. Figure 8 shows the average power spectrum of this “interpulse” region during this time interval, and confirms the initial claims of Israel et al. (2005) that signals at  $\approx 30$  and 92 Hz are present towards the end of the hyperflare. These QPOs are extremely significant, for example, we conservatively estimate the significance of the 30 Hz QPO at  $1.4 \times 10^{-11}$ , and the 90 Hz feature is even more significant. These QPOs can be fitted with lorentzian profiles. Based on such fits we find centroid frequencies of  $28.98 \pm 0.4$ , and  $92.9 \pm 0.2$  Hz; quality factors ( $\nu_0/\Delta\nu$ ) of  $7 \pm 0.8$ , and  $39 \pm 5$ ; and average amplitudes of  $20.5 \pm 3$  %, and  $19.2 \pm 2$  %, respectively.

The 30 Hz feature in the RXTE spectrum is far more significant than the weaker feature at 30 Hz found in the RHESSI spectrum. This is at first glance surprising, since RHESSI has a higher countrate once the rear segments are included. There are however several factors that probably contribute to this discrepancy. Firstly, we are in the interpulse region, where RHESSI’s high background levels are more important. Secondly, one cycle of this time period was excised from the RHESSI data because of an artificial spike in countrate as a protective attenuator was removed. In addition, as discussed above, we find occasions where the 26 Hz QPO appears far more prominently in the RXTE data than in the RHESSI data, suggesting that other factors such as scattering off the spacecraft and the Earth may reduce RHESSI’s effectiveness and offset the higher countrate.

## 2.4. Amplitude variation and frequency drift

In the periods when they are detected, the QPOs are far from static. Their amplitudes wax and wane, and there is evidence for frequency shifts and possible multiplet splitting. In Figure 9 we show a sequence of dynamical power spectra for the Peak 2/Interpulse region, for the time period when the 92.5 Hz QPO is active. The presence of the strong QPO at this frequency from 180-230s after the main flare is clear (Panels 17-24 of Figure 9). If we look at the cycles around this period however, there are hints of interesting behavior. Back at only 80s after the flare, weak detections are made, with a frequency that starts at around 78 Hz and rises up to a strong 92.5 Hz QPO that persists for a couple of cycles from 120-130 s. The QPOs then weaken, and the frequency seems to fall again by a few Hz, until the strong 92.5 Hz signal reappears at 180s. At later times, as already noted by Israel et al. (2005), the frequency rises to 95 Hz and possibly higher, as the amplitude falls and the signal becomes undetectable.

The variation of amplitude over the rotational cycle, and the consequent interruption of the signals, means that we cannot rigorously connect cycles, as one would wish to in order to verify that the frequency is evolving. However, our results are suggestive of this eventuality. There is also some suggestion of frequency movement in the lower and higher frequency QPOs (see for example Figure 3), although this is even harder to track from cycle to cycle because the QPOs are weaker and the amplitudes more variable. As such it is not possible to verify whether the other QPO frequencies move in concert with the 92.5 Hz QPO.

## 3. Discussion

Using phase averaging techniques we have found evidence for additional, higher frequency QPOs during the December, 2004 hyperflare from SGR 1806-20. The properties of the QPOs, reported in this and previous papers, are summarized in Table 1 and Figure 10. The additional frequencies and the time and phase dependence of the detections suggest an extremely rich and complex phenomenology associated with the magnetar oscillations.

The detection of a strong 625 Hz QPO in the RXTE data is particularly interesting. The frequency is remarkably similar to that of a QPO found by us in the RHESSI data, but there are some intriguing differences in the properties of the two QPOs. In addition to having a slightly lower centroid frequency (there is frequency overlap of the QPO profiles however), the RXTE QPO has substantially lower fractional amplitude and coherence value  $Q$ . The RXTE QPO appears later in the tail of the flare, and the apparent photon energies of the two QPOs also differ.



The RHESSI detection used events from the front segments, in the 100 - 200 keV energy band (see Watts & Strohmayer (2006) for a discussion of RHESSI data in this context). The phase interval was centered on the rising edge of peak 1 (Watts & Strohmayer (2006), Figure 4), and the average was obtained from about 50 to 200 s after the start of the hyperflare. An average power spectrum from RXTE for the same time and phase ranges shows no corresponding signal in the PCA. However, it is difficult to know exactly how to compare the energies of events detected in the two instruments. For RHESSI, many of the events observed in the front segments were direct (ie. meaning that they were not scattered before detection), whereas this is likely not the case with RXTE, as virtually no photons would have made it directly into the PCA xenon volumes without having scattered off of some part of the spacecraft. It is quite possible that no photons with incident energies in the 100 - 200 keV range were detected by the PCA, which would account for the non-detection. The later, lower amplitude RXTE QPO is not detected in the RHESSI data, most probably due to the lower countrates.

The lack of simultaneous detections is therefore disappointing, but not surprising. Perhaps more important is the fact that the two instruments detected signals independently at consistent frequencies. The QPO profile of the 625 Hz feature detected with RXTE overlaps the 1 Hz bin (centered on 626.5 Hz) in which the signal was detected with RHESSI. Although it is difficult to determine an *a priori* probability, it seems extremely unlikely that both instruments would detect signals at a consistent frequency unless that frequency were intrinsic to the source. We therefore think there is compelling evidence to associate this frequency with SGR 1806-20.

The finding of additional characteristic frequencies in the SGR 1806-20 hyperflare further strengthens the connections between the oscillations seen in both the SGR 1806-20 and SGR 1900+14 events. In each case, oscillations near  $\approx 30$ ,  $\sim 90$  and  $\approx 150$  Hz have been seen. This strongly supports the notion that the same physical processes are involved in these objects.

Several mechanisms have been suggested as the cause of the QPOs. One suggestion is that the QPOs are caused by an interaction with a remnant or ejected debris disk, the mechanism being similar to that which gives rise to the kHz QPOs in accreting neutron stars. Although there is now evidence that some magnetars have disks (Wang, Chakrabarty & Kaplan 2006), there is no evidence as yet for a disk around the SGRs, and it is also very difficult to understand the rotational phase dependence if a disk is responsible.

An alternative is that we are seeing oscillations of the plasma-filled magnetosphere and the trapped fireball. Simple estimates of the Alfvén speed in the magnetosphere suggest that magnetospheric frequencies would be too high to explain the observations, but evolution of

the magnetosphere and fireball over the course of the tail might be a natural explanation for the frequency drift suggested in Section 2.4. The theoretical details of such modes remain to be worked out, however, and we will not discuss the magnetospheric model further in this paper. We will instead focus on the third and perhaps most promising mechanism, neutron star vibrations.

### 3.1. Neutron star oscillations

The detection of similar frequencies in SGR 1806-20 and SGR 1900+14 makes sense in the context of global oscillation modes; if the neutron stars have similar masses and magnetic fields, then they should ring with the same set of characteristic frequencies. The detection of similar frequencies at different rotational phases (the  $\approx 625$  Hz QPOs) also argues in favor of an underlying global oscillation, with magnetospheric beaming/obscuration effects causing the phase dependence. Frequency drift can also be incorporated within this model, as discussed later.

Attention has so far focused on the toroidal shear modes of the neutron star crust, thought to be both easy to excite and strongly coupled to the external magnetosphere (providing a means to modulate the X-ray lightcurve). The most detailed computations of mode frequencies to date have included both the depth-dependence of the shear modulus within the crust, and the effective boost to the shear modulus due to the magnetic pressure (Duncan 1998; Piro 2005). Potentially important effects that have not been addressed in detail include coupling between crust and core due to the magnetic field, the equation of state in the boundary layer between crust and core, and non-uniformity of the magnetic field. In what follows we will refer to the models that assume no coupling between crust and core as “pure crust” models; and those that do include coupling due to the field as “coupled crust-core” models.

The question of whether or not “pure crust” models are adequate is an important one. Levin (2006) used a toy model to show that if there is a strong perpendicular magnetic field threading the boundary, then large horizontal displacements at the base of the crust must excite vibrations in the core. The effects of coupling may however be mitigated in several ways. For example, coupling to the core will depend sensitively on the amplitude at the crust core boundary, and previous calculations show that this amplitude can be substantially smaller than that at the top of the crust (see McDermott, van Horn & Hansen 1988, for example). Thus, approximating the amplitude as a single constant for a given mode, as assumed by Levin, may not be very accurate. The physics at the boundary layer at the base of the crust will also be crucial (see for example Kinney & Mendell (2003)).

The elastic properties at the base of the crust (Pethick & Potekhin 1998) have not yet been considered, and could substantially modify the eigenfunctions in this region. In addition, coupling will likely depend rather sensitively on both the magnetic field geometry and the particular displacement pattern of individual modes. The modes that persist, and that we observe, may be those for which the coupling is minimal. The presence of a strong toroidal field in the core of the star could also reduce coupling by making core more rigid and less prone to excitation.

We will return to the issue of coupling later in this Section. For the moment, however, we will start by assessing the observations in the light of the “pure crust” models.

### 3.2. Interpretation as “pure crust” modes

The 30 Hz, 92 Hz and 150 Hz QPO can be interpreted within the global oscillation model as  $n = 0$ ,  $l=2$ , 7 and 12 torsional modes of the neutron star crust. Watts & Strohmayer (2006) suggested that the 626 Hz oscillation seen in RHESSI data could be associated with a toroidal mode having a single node in the radial displacement eigenfunction ( $it_1$  modes). Recent estimates from Piro (2005, see his Figure 3) suggest that this frequency is consistent with theoretical expectations. Our confirmation of the same frequency in the RXTE data, provides a firm indication that we are seeing not only modes with a sequence of different  $l$ -values, but also modes with different  $n$ -values.

It is possible that the 625 Hz QPO seen in the RXTE dataset represents an evolution of the QPO seen earlier in the flare in the RHESSI data. However, the mode model also offers a possible explanation for the detection of two  $\approx 625$  Hz QPOs with differences in properties. Calculations (see Hansen & Cioffi (1980); Piro (2005)), indicate that the  $n = 1$  mode frequencies are not very sensitive to  $l$ . As such we could be seeing two  $n = 1$  modes of different  $l$ , excited at different times by either aftershocks or mode coupling. The implications of detecting an  $n = 1$  mode are discussed in more detail in Section 3.2.1.

The 18 Hz and 26 Hz QPOs are at first glance too low in frequency to fit simple torsional mode models, however, mode calculations with realistic magnetic fields will have  $m$ -dependent splitting, perhaps producing an observable multiplet structure. This might accommodate the observed spread from about 26 - 30 Hz in a putative  ${}_2t_0$  mode, but detailed calculations will be required to explore this quantitatively. The 18 Hz QPO, however, remains difficult to understand.

The stronger high frequency QPOs at 625 and 1840 Hz can be nicely accommodated within the torsional mode hypothesis as low  $l$ ,  $n = 1$  and  $n = 3$  modes, respectively (see, for

example, Figure 3 in Piro 2005). The less significant features at 720, 976, and 2,384 Hz, may also fit within this scenario. The 720 Hz might represent a low  $n$  mode with significantly different  $l$ , as pointed out by Hansen & Cioffi (1980), the  $l$  dependence of such modes is not strong, but can produce a scatter in frequency on the order of 15%. The other frequencies might correspond to modes with  $n = 2$ , and  $n > 3$ , respectively. In addition, at these high frequencies, other modes, such as the crustal spheroidal modes (see McDermott et al. 1988), may become relevant. Again, more detailed mode calculations, including the effects of magnetic fields, will be needed to make more quantitative mode identifications.

### 3.2.1. Implications for Neutron Star Crusts

If the 625 Hz QPOs are indeed  $n = 1$  torsional modes, the implications for the study of neutron star structure are profound. The ratio of frequencies of the  $n = 1$  and  $n = 0$  torsional modes enables one to deduce the depth of the neutron star crust (see Hansen & Cioffi 1980; Piro 2005). The basic physics behind this estimate is that the  $n = 0$  mode frequencies are set by the horizontal wavelength, which scales with the stellar radius,  $R$ , whereas the  $n > 0$  mode frequencies are dominated by the vertical wavelength, which senses the depth of the crust,  $\Delta R$ . In the limit of a thin crust and a constant shear wave speed, one finds the simple expression (see Hansen & Cioffi 1980; McDermott et al. 1988; Piro 2005),

$$\frac{\nu_{l,n=0}}{\nu_{n>0}} = \frac{(l(l+1))^{1/2}}{3n} \frac{\Delta R}{R} . \quad (1)$$

If we identify 30 Hz with the  $l = 2$ ,  $n = 0$  mode frequency, and 625 Hz with the  $n = 1$  mode (and  $l \approx n$ ), the above expression predicts  $\Delta R/R = 0.06$ . In most modern neutron star models, however, the crust is not “thin” in the sense of  $\Delta R/R \ll 1$ , and the shear speed has some variation with depth, so this simple estimate should probably be considered a lower limit. A more accurate estimate can be obtained by comparisons with more detailed mode calculations. For example, using the calculations of McDermott et al. (1988) we evaluated the expression,  $(\nu_{l,1}\Delta R)/(\nu_{2,0}R)$ , that according to the approximate theory should be the proportionality constant between the mode frequency ratio and the fractional depth of the crust. For the four models tabulated by McDermott et al. (1988) we find that this expression ranges from 2.15 to 2.65. Adopting this range as representative, and using the scale factors to convert our observed mode frequency ratios into depths, we obtain the range,  $0.1 < \Delta R/R < 0.127$ . We note that the models from McDermott et al. use softer equation of state models than are currently favored, so it is important to repeat this exercise with more up to date neutron star models, and also incorporate magnetic fields. In addition the effects of possible crust-core coupling must be considered (see next subsection).

Measuring the thickness of a neutron star crust also conveys information on the equation of state (EOS). In other words, stellar models of a given mass computed with different EOSs will in general have crusts of different depths. For example, Lattimer (2006) has recently outlined how constraints on the fractional depth and stellar mass could be used to constrain the nuclear symmetry energy and the nuclear force model. The crust depth dependence on the EOS also has implications for pulsar glitch models (see, for example, Crawford & Demianski 2003; Link, Espstein & Lattimer 1999).

### 3.3. Coupled crust-core modes

If the coupling between crust and core is strong, by virtue of boundary layer physics or magnetic field threading, one needs to consider the global magneto-elastic modes of the neutron star. As first suggested by Israel et al. (2005), global modes can accommodate the lower frequency 18 and 26 Hz QPOs very easily. A recent paper by Glampedakis, Samuelsson & Andersson (2006) developed a simple slab model of global magneto-elastic oscillations that showed two interesting features. Firstly, it confirmed the presence of modes at lower frequencies than the “pure crust” toroidal modes. Secondly, the model exhibited modes for which the amplitudes in the crust were strong; in these cases the frequency was very close to the well-established “pure crust” frequencies. In other words, even with coupling included, it is possible to obtain very similar frequencies to those that we know match the data. Although the model was very simple (slab geometry, for example, is not adequate to describe behavior deep in the core), this gives us some indication that global modes may have similar frequencies. Low core amplitudes would also reduce damping, another issue of concern for Levin (2006)<sup>1</sup>. The bounds on crust thickness estimated in section 3.2.1 above were based on “pure crust” models. In principle, however, a similar calculation could be done for coupled crust-core modes, using the ratio of two frequencies to scale out gravitational redshift effects.

---

<sup>1</sup>The toy model developed by Levin possesses a continuous spectrum of apparently singular modes in the core fluid that he claims will drain energy from the system, leading to rapid damping of global oscillations. Firstly, the continuous spectrum in his problem is a consequence of the unbounded geometry and simplified assumptions of the toy model; whether such a continuum would exist in a realistic stellar model is not yet clear. Secondly, an apparently singular continuous spectrum of eigenfunctions can form a non-singular collective perturbation when one considers the initial value problem (the response to an initial perturbation such as a crust fracture). The temporal behavior and response to damping of such a perturbation is far from straightforward (Watts et al. 2003; Watts, Andersson & Williams 2004). As such we think Levin’s conclusions regarding the lifetimes of global oscillations are premature.

### 3.4. Temporal variation

Figure 10 shows the periods during the tail of the flare when the different QPOs are detected in either the RXTE or RHESSI datasets. Some of the oscillations are seen throughout the flare, others are detected only after the rise in emission half way through the tail, and the highest frequency modes are very short-lived. This complex temporal variation requires explanation, and to do this we must understand the excitation and damping mechanisms.

The data suggest that some QPOs are excited by the main flare, whereas others are excited later in the tail, perhaps by aftershock fracturing and reconnection, or energy release from the core. The association of several of the QPOs with the rise in emission late in the tail lends support to the idea of continued excitation. However, there remains the possibility that all of the QPOs are excited by the main flare, with their visibility depending on beaming effects that vary during the tail. Beaming will be influenced by both the magnetic field and by the plasma surrounding the magnetar. Selection by beaming might also account for the fact that only some of the myriad oscillations predicted by theory are observed - although mode excitation will also depend sensitively on the speed and extent of the fracture. Some modes may also damp far too quickly to be detected, depending on local conditions in the crust and magnetic field geometry. We believe that these factors are more than capable of accounting for the fact that only a few frequencies reach detectable amplitudes, an issue of concern to Levin (2006).

Once a mode is excited, there is still significant variation in amplitude and perhaps in frequency (as discussed in Section 2.4). One possibility to explain amplitude variation is that the mechanism which modulates the X-ray flux is strongly “tunable.” That is, at times when certain frequencies are detected their instantaneous amplitudes can be quite high, almost certainly higher than the relative surface motions. So, it may be that the modulation mechanism can amplify relatively small surface motions. Resonant interaction between the crust and the core could also lead to amplitude variations over the course of the tail. Frequency drifts could arise in several ways. Evolution of the magnetic field in the aftermath of the flare, relaxation of the deep crustal structure, and the evolution of the surrounding plasma, are all candidates for causing frequency shifts. Alternatively we could be seeing different members of a magnetically-split multiplet excited, perhaps, by mode coupling.

#### 4. Conclusions

Our study of the RXTE data from the SGR 1806-20 hyperflare indicates that a complex pulsation phenomenology is associated with magnetar hyperflares. The discovery of new kHz-range frequencies consistent with theoretical predictions for  $n > 0$  torsional modes provides strong evidence that we may be seeing vibration modes of the neutron star crust excited by these catastrophic events. If this is true, then it opens up the exciting prospect of probing the interiors of neutron stars in a manner analogous to helioseismology. Additional excitement is warranted when we consider that all the current datasets used to explore these oscillations have been purely serendipitous. That is, they have not been optimized in any way for studying these signals. This suggests that a wealth of additional information would likely be found from instruments better optimized to capture with high time resolution the flood of X-rays produced by these events. Based on the findings presented here we are also strongly convinced that more theoretical work is definitely needed to make more accurate mode identifications, to better understand the excitation and damping mechanisms of modes and how they can couple to the X-ray emission, and to make more precise inferences on neutron star structure.

ALW acknowledges support from the European Union FP5 Research Training Network “Gamma-Ray Bursts: An Enigma and a Tool”. TES thanks NASA for its support of high energy astrophysics research. We are also grateful to the anonymous referee for a detailed report, including many useful thoughts on QPO interpretation.

#### REFERENCES

- Crawford, F., & Demiański, M. 2003, *ApJ*, 595, 1052.
- Duncan, R.C. 1998, *ApJ*, 498, L45
- Flowers, E., & Ruderman, M.A. 1977, *ApJ*, 215, 302
- Glampedakis, K., Samuelsson, L. & Andersson, N. 2006, *astro-ph/0605461*
- Hansen, C. J. & Cioffi, D. F. 1980, *ApJ*, 238, 740.
- Israel, G., et al., 2005, *ApJ*, 628, L53
- Kinney, J.B., & Mendell, G. 2003, *Phys. Rev. D*, 67, 024032

- Lattimer, J. M. 2006, to appear in the Proceedings of the conference ‘Isolated neutron stars: from the interior to the surface’, published in ApSS (Springer)
- Levin, Y. 2006, MNRAS, 368, L35.
- Link, B., Epstein, R. I., & Lattimer, J. M. 1999, Physical Review Letters, 83, 3362.
- McDermott, P.N., van Horn, H.M., & Hansen, C.J. 1988, ApJ, 325, 725
- Pethick, C.J. & Potekhin, A.Y. 1998, Phys. Lett. B, 427, 7
- Piro, A.L. 2005, ApJ, 634, L153
- Schwartz, S.J., et al. 2005, ApJ, 627, L129
- Smith, E., Swank, J., Markwardt, C.B., Rephaeli, Y., Gruber, D., Persic, M., & Rothschild, R., 2005, GCN GRB Observation Report 2927
- Strohmayer, T.E., & Watts, A.L. 2005, ApJ, 632, L111
- Thompson, C., & Duncan, R.C. 2001, ApJ, 561, 980
- Thompson, C., & Duncan, R.C. 1995, MNRAS, 275, 255
- Wang, Z., Chakrabarty, D., & Kaplan, D.L. 2006, Nature, 440, 772
- Watts, A.L., Andersson, N., Beyer, H. & Schutz, B.F. 2003, MNRAS, 342, 1156
- Watts, A.L., Andersson, N. & Williams, R.L. 2004, MNRAS, 350, 927
- Watts, A.L. & Strohmayer, T.E. 2006, ApJ, 637, L117



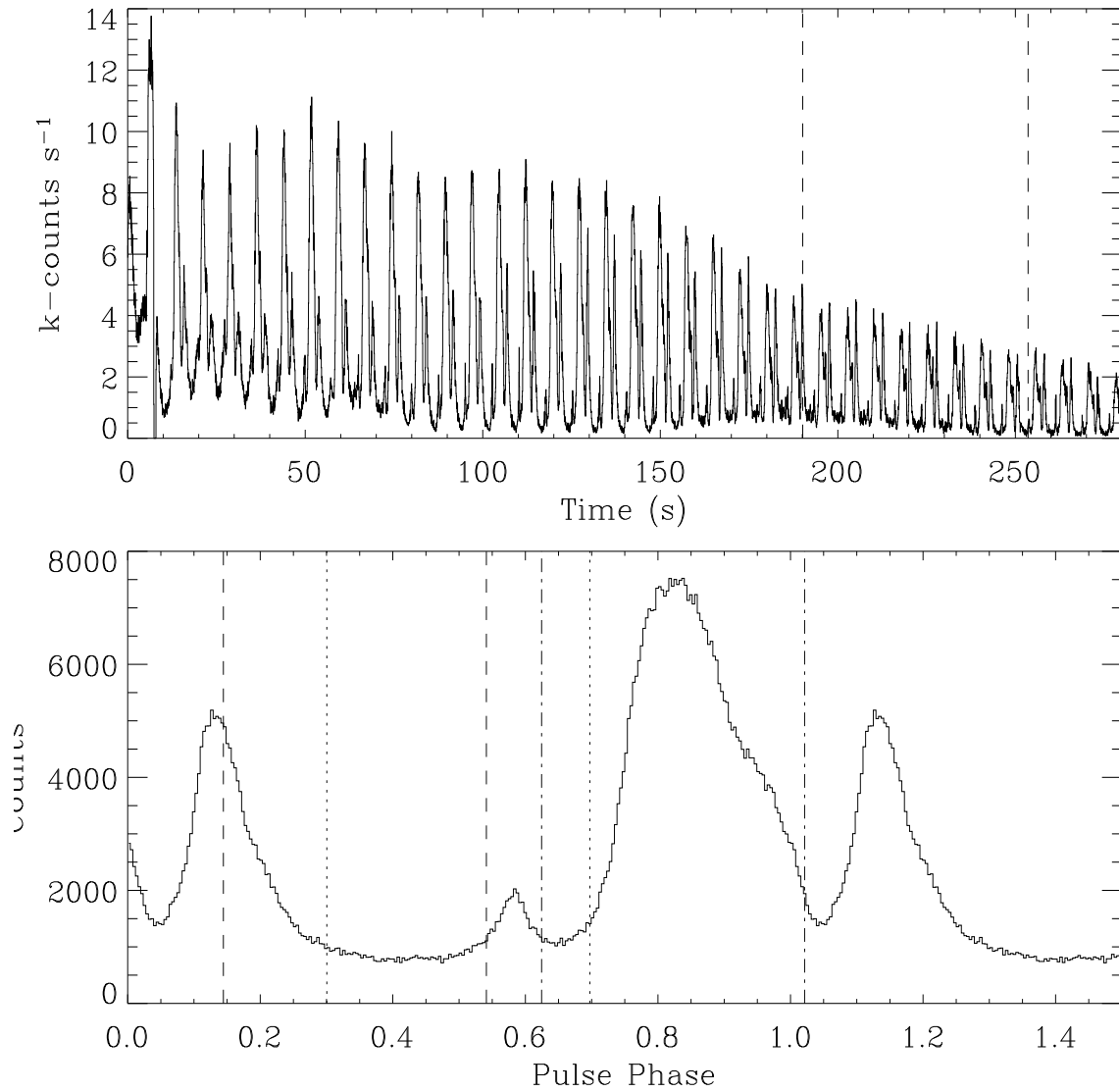


Fig. 1.— X-ray intensity of the December, 2004 hyperflare as measured by the PCA (top), and the average pulse profile (bottom). The curves include all good events detected in PCA channels 10 - 200 (nominal energy band from 4 - 90 keV). The main flare takes place approximately 4s prior to the zero on the time scale. The time interval in which the 625 Hz oscillation was detected is marked by the vertical dashed lines (top). The vertical lines in the bottom plot denote the phase ranges used to compute power spectra shown in Figures 2, 4 and 5 (dashed), 6 (dash-dot), and 7 (dotted). The text refers to Peaks 1, 2 and 3: Peak 1 is at phase  $\approx 0.8$ , Peak 2 at  $\approx 0.1$  and Peak 3 at  $\approx 0.6$ .

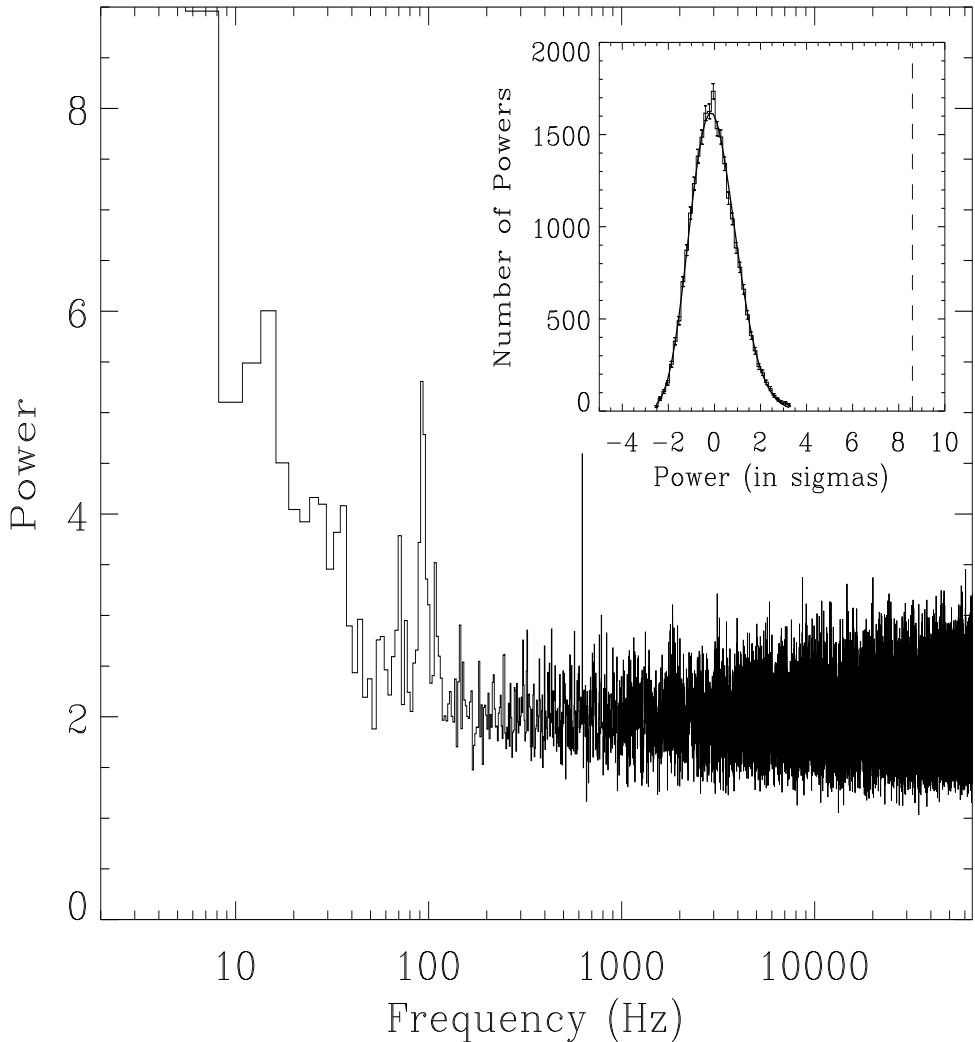


Fig. 2.— Average power spectrum from a portion of the hyperflare from SGR 1806-20 (main panel). We averaged nine 3 s power spectra from the time interval marked by the vertical dashed lines in Figure 1 (top). The frequency resolution is 2.66 Hz. The inset panel shows the distribution of noise powers computed from the frequency range 800 - 65,536 Hz as well as the best fitting  $\chi^2$  distribution (solid). The distribution is plotted in units of  $\sigma$ 's. The vertical dashed line marks the peak power of the 625 Hz feature. See the text for further discussion.

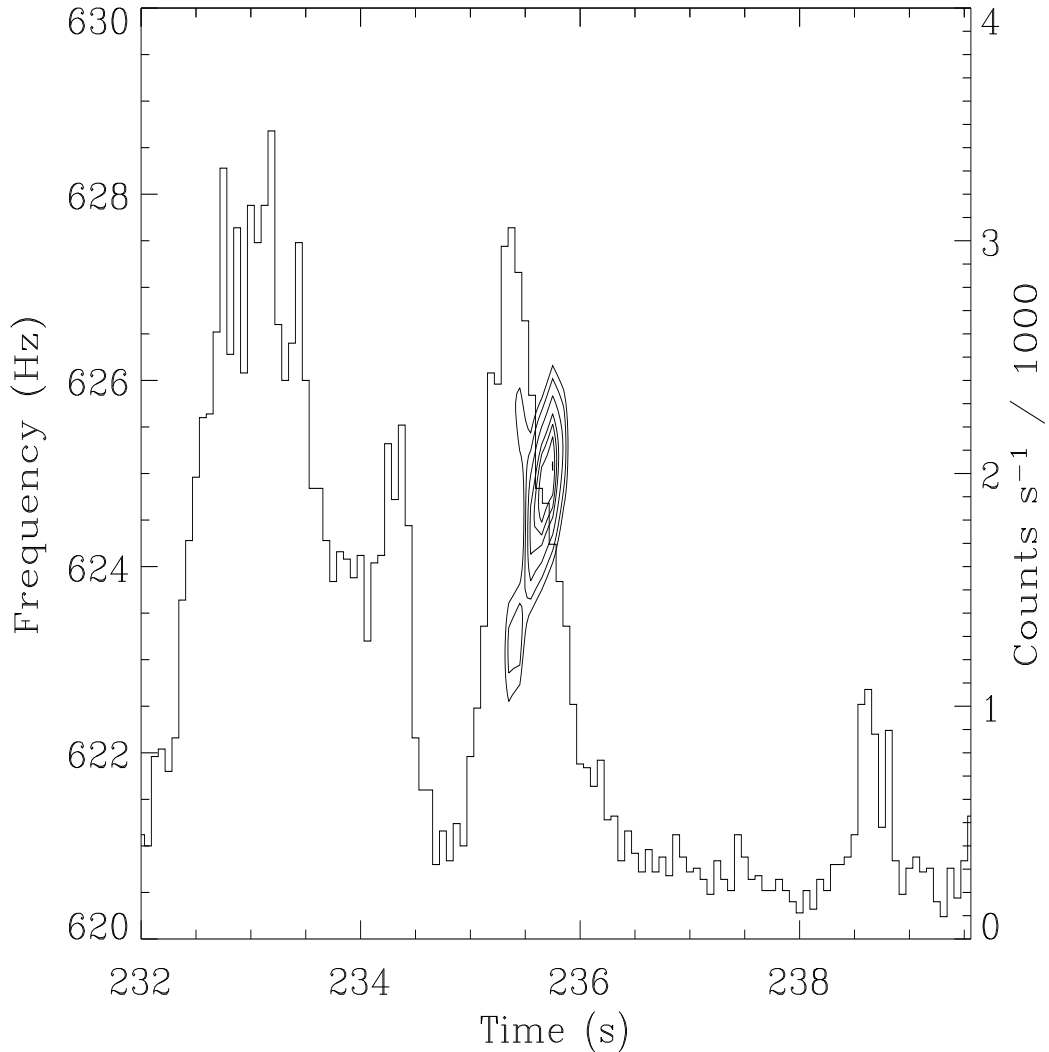


Fig. 3.— Dynamic power spectrum of a portion of the data interval in which the 625 Hz oscillation was detected. Contours of constant Fourier power are plotted as a function of frequency and time, along with the X-ray intensity as a function of time. We used 0.5 s intervals to compute the power spectra, and overlapped the intervals, beginning a new one every 0.1 s. A strong contribution to the 625 Hz signal detected in the average power spectrum of Figure 1 is evident on the falling edge of peak 2. Contours at Leahy normalized power levels of 16, 18, 20, 24, 28 and 32 are shown. A single rotational cycle is plotted.

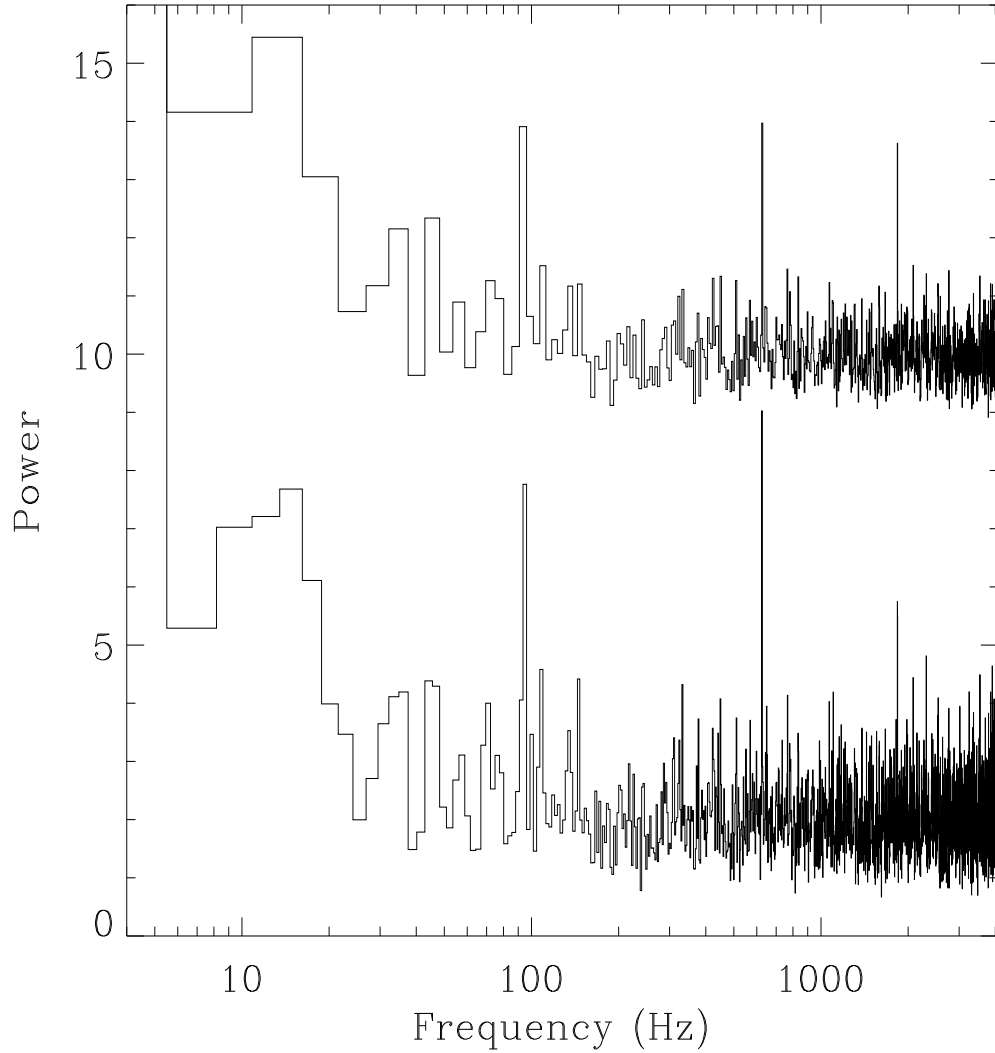


Fig. 4.— Average power spectrum from two consecutive cycles beginning with the cycle immediately prior to the pulse displayed in Figure 3 which shows a strong 625 Hz signal. Two representations of the same power spectrum are shown, only the frequency resolutions differ. The frequency bins are 2.667 Hz wide in the bottom trace and twice that in the top. Three frequencies are prominent in the top trace, 92 Hz, 625 Hz, and 1,840 Hz. See the text for additional discussion.

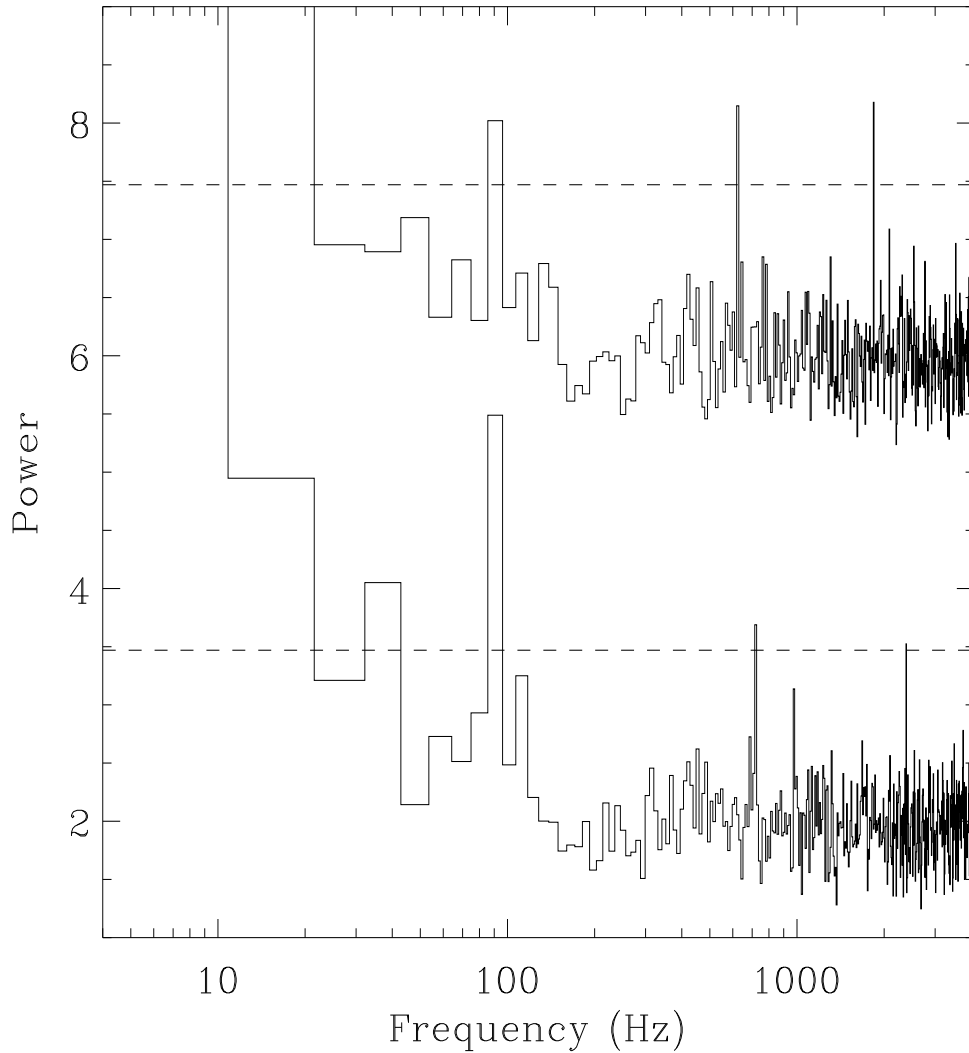


Fig. 5.— Average power spectra from the time interval in which the 625 Hz oscillation was first detected. Shown are average power spectra computed from two consecutive cycles. The top panel includes the pulsation cycle shown in Figure 3, and the preceding cycle (same as in Figure 4, only plotted with lower frequency resolution). The bottom panel shows the spectrum from an earlier, 2-cycle time interval, beginning six cycles before that shown in Figure 3. In each case the frequency resolution is 10.66 Hz. In each spectrum a horizontal dotted line marks a  $4\sigma$  (one trial) deviation. The 625 and 1,840 Hz features are detected in the top spectrum, while several different frequencies are suggested in the bottom spectrum. See the text for more details.

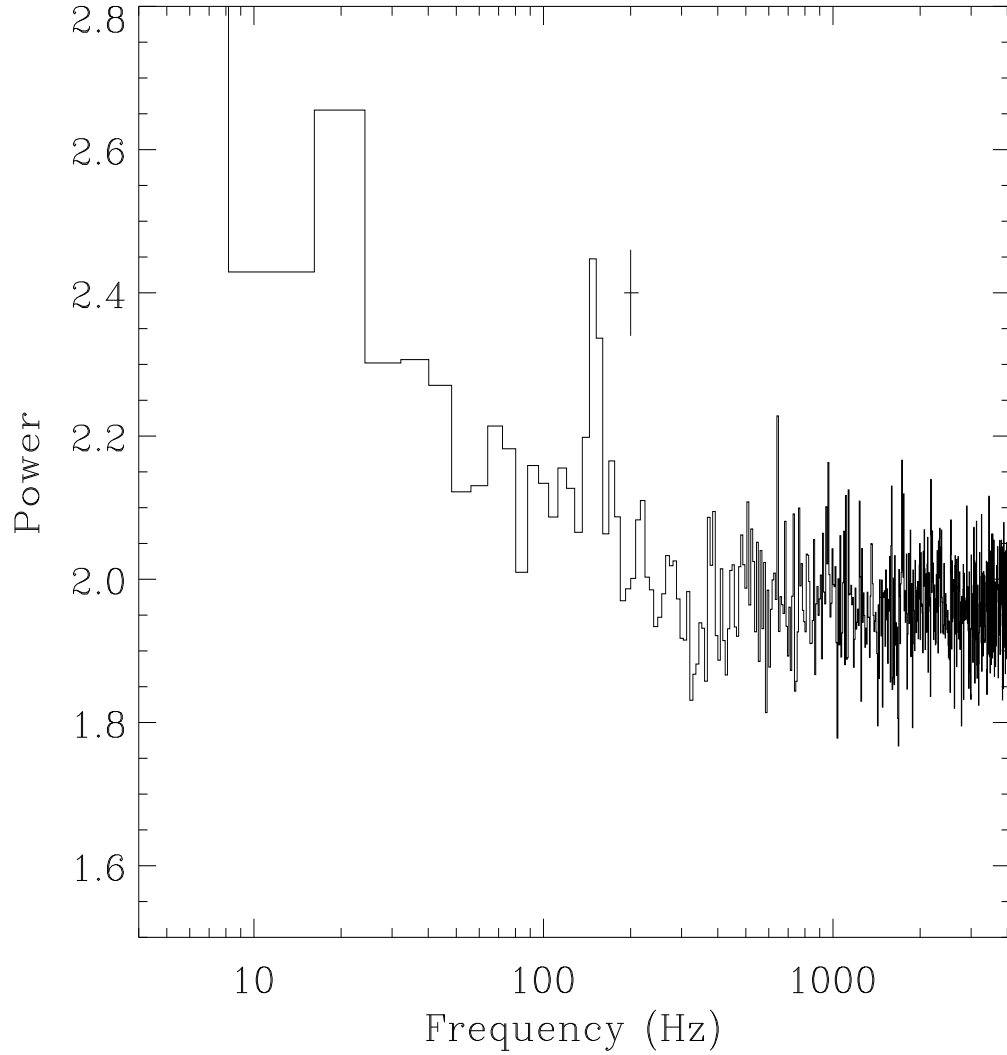


Fig. 6.— Average power spectrum of the phase region centered on peak 1, showing the 150 Hz QPO. We averaged 45 power spectra, each computed from 3 s of data over essentially the entire flare. The phase interval used is shown by the vertical dot-dashed lines in Figure 1. A characteristic error bar is shown next to the QPO peak.

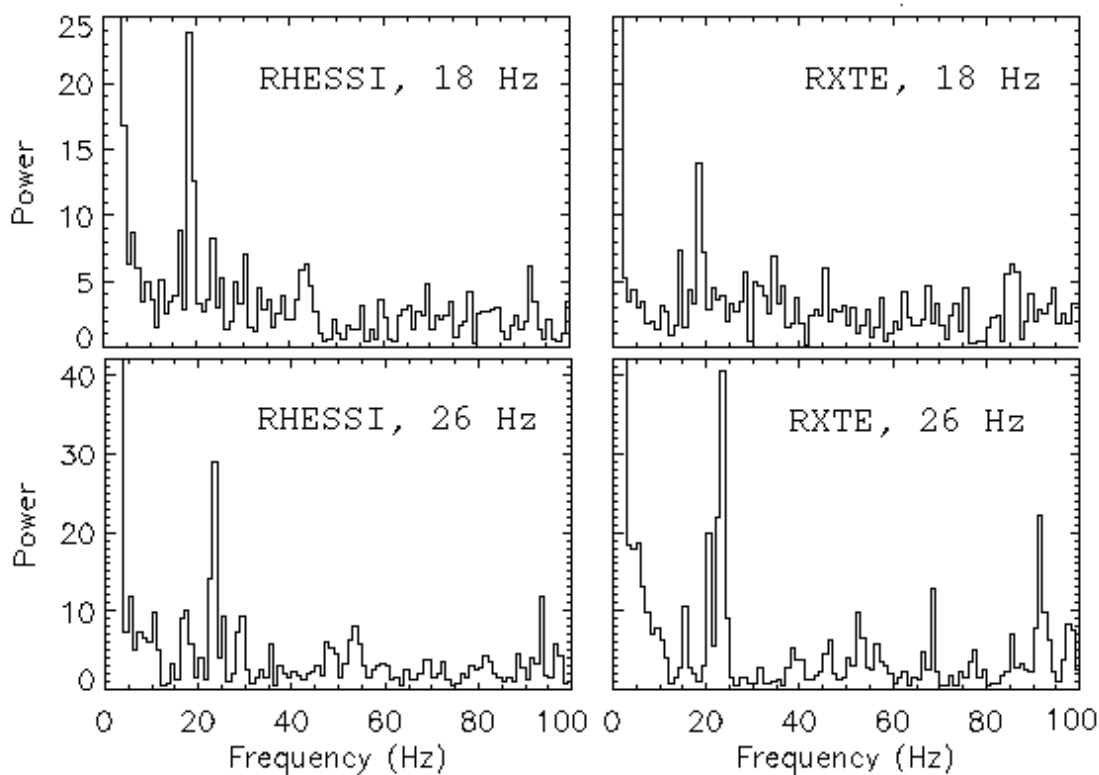


Fig. 7.— Average power spectra computed for RXTE and RHESSI data, for one cycle in which either the 18 Hz or the 26 Hz QPO is particularly strong in the RHESSI dataset. Each power spectrum has 1 Hz frequency resolution, and is computed using 0.3 rotational cycles. The interval shown for the  $\approx 18$  Hz QPO starts 89s after the main flare; that for the  $\approx 26$  Hz QPO Starts 127s after the main flare. Simultaneous peaks are seen in the RXTE data despite the apparent countrate disadvantages of RXTE.

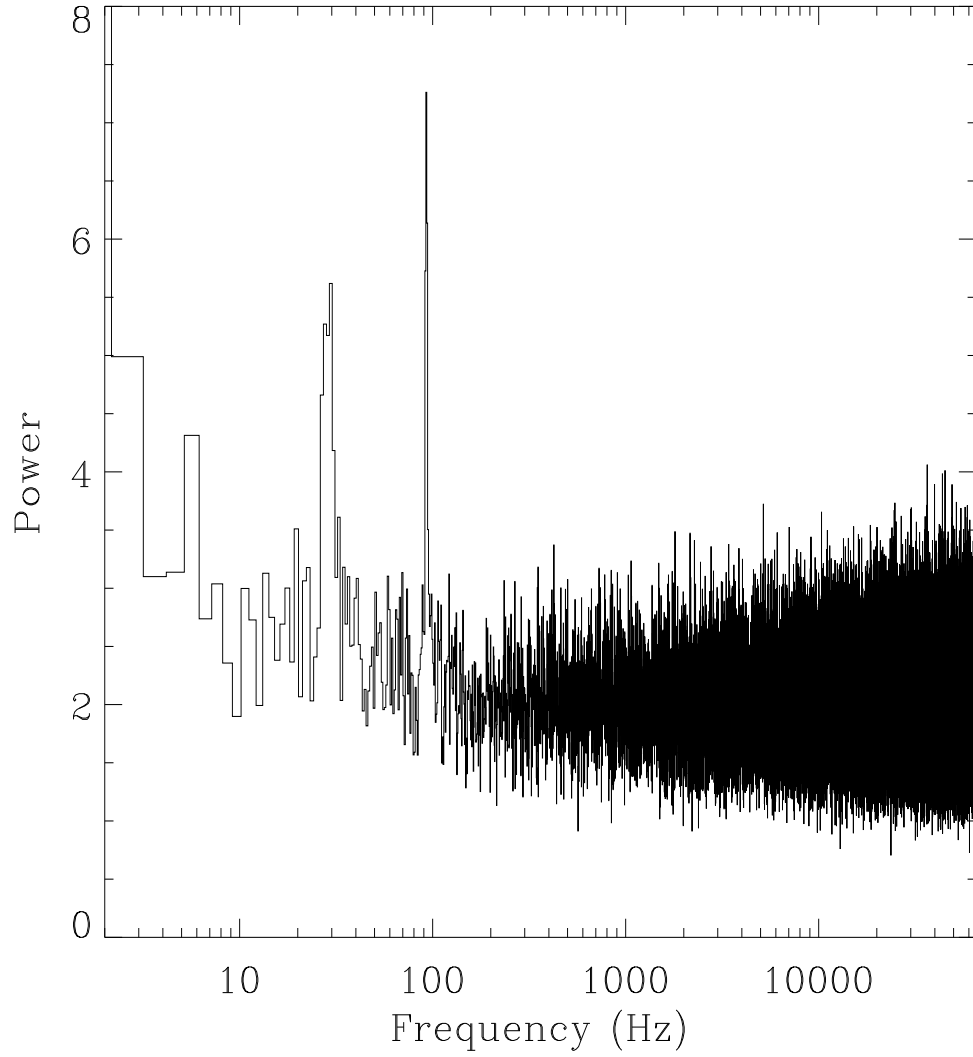


Fig. 8.— Average power spectrum from the “interpulse” region during the same time interval in which the 625 Hz oscillation was detected. The phase interval used for the average spectrum is marked with vertical dotted lines in Figure 1. Strong QPOs at 29 and 92 Hz are clearly detected. See the text for additional discussion.



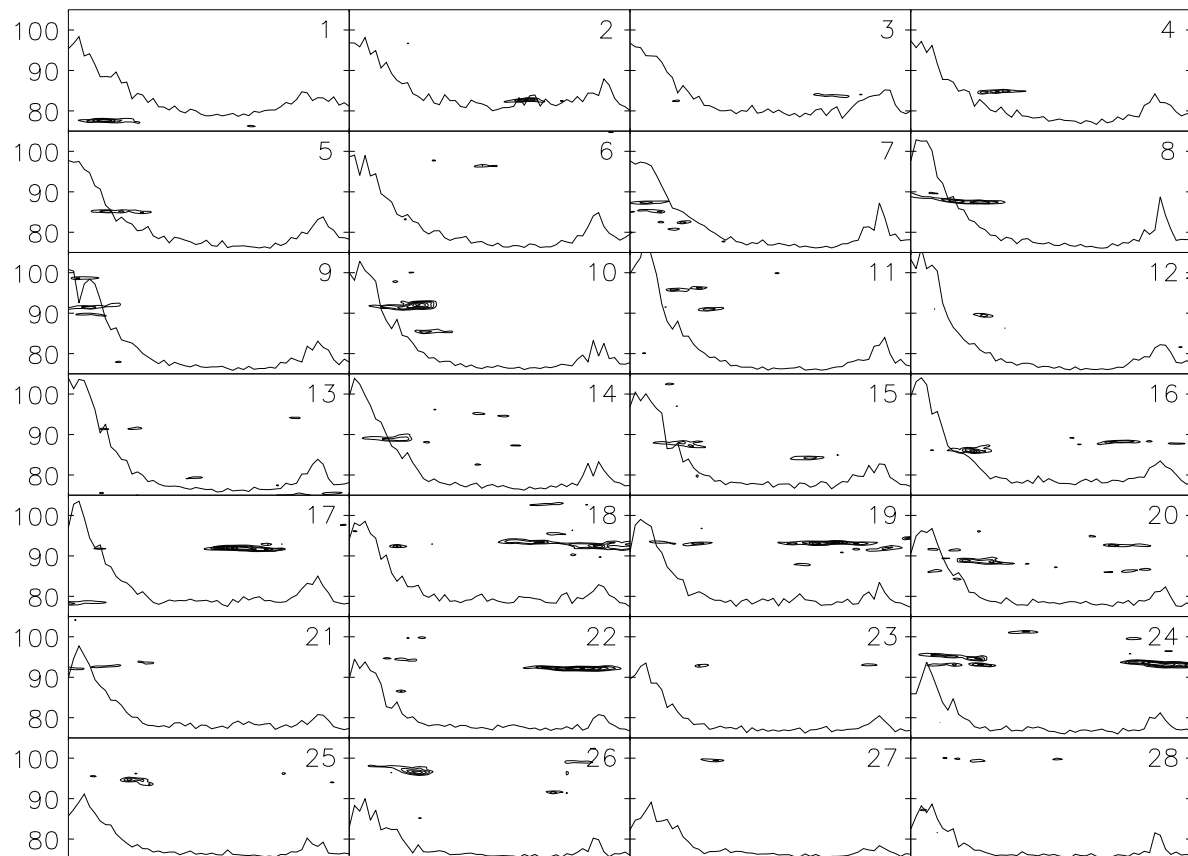


Fig. 9.— The evolution of frequency in the 75-105 Hz band, for the Peak 2/interpulse region. Each numbered panel shows a 4s interval for consecutive cycles, the first panel starting  $\approx 60$  s after the main flare. The y-axis shows frequency in Hz. Dynamical power spectra, shown as contours, are computed from 1s segments, overlapping by 0.1s. The minimum contour level shown is a power of 15, with increments of 5. Lightcurves are also shown, plotted to the same scale on each panel. The plots show amplitude variation, frequency evolution, and possible multiplet activity. The start time of each panel in seconds (relative to the initial flare at time zero) is: (1) 59.8, (2) 67.4, (3) 75.0, (4) 82.5, (5) 90.1, (6) 97.7, (7) 105.3, (8) 112.8, (9) 120.4, (10) 128.0, (11) 135.6, (12) 143.1, (13) 150.7, (14) 158.3, (15) 165.9, (16) 173.4, (17) 181.0, (18) 188.6, (19) 196.2, (20) 203.7, (21) 211.3, (22) 218.9, (23) 226.5, (24) 234.0, (25) 241.6, (26) 249.2, (27) 256.8, (28) 264.3

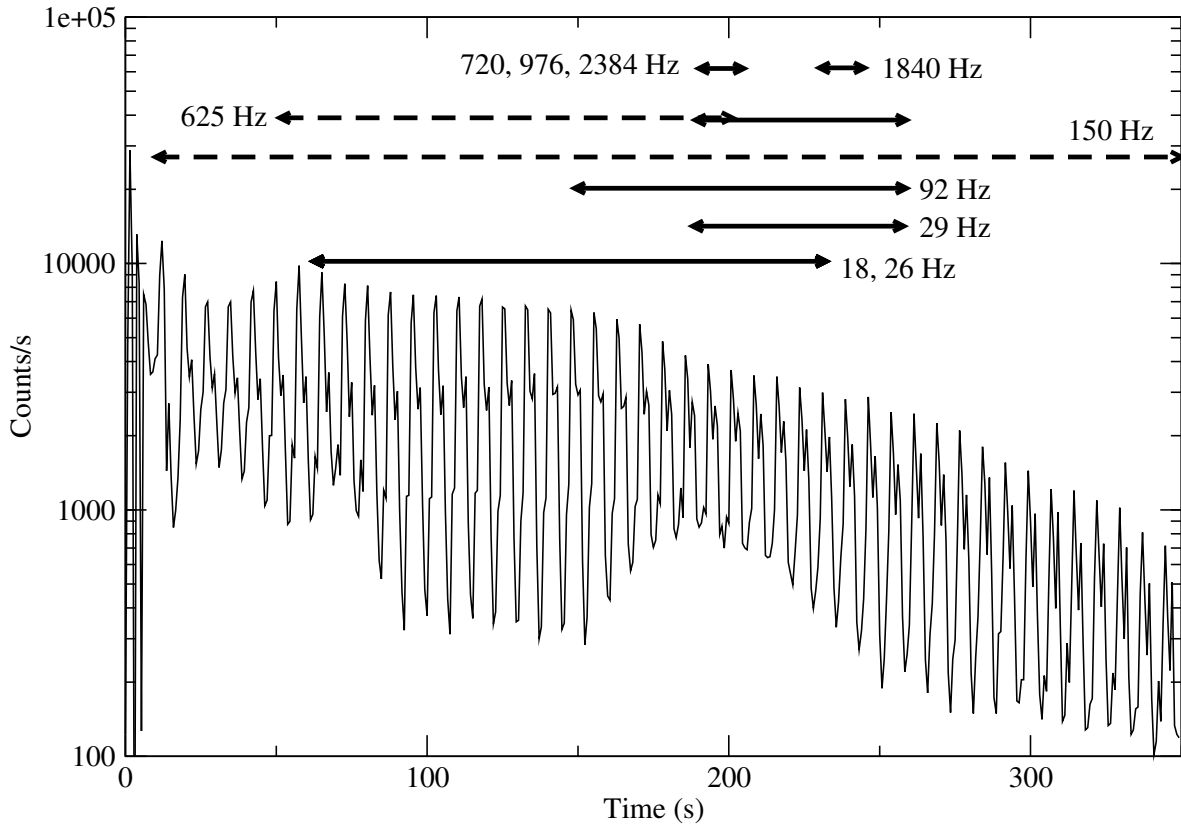


Fig. 10.— The time periods when the different QPOs are detectable in either the RXTE or RHESSI datasets. Solid lines indicate QPOs that are detected in the Peak 2/Interpulse region. Dashed lines indicate QPOs that are detected primarily during Peak 1. The difference in properties between the two  $\approx 625$  Hz QPOs, the earlier one detected by RHESSI and the later one by RXTE, is clear.

Table 1. Summary of properties for the most significant QPOs detected in the tail of the SGR 1806-20 giant flare. The frequency is the centroid frequency from a Lorentzian fit; the quoted width is the associated full width at half maximum. All amplitudes are the values computed from rotational phase dependent power spectra. The duration is given with respect to the main flare at time zero. For the phase, P2/I indicates that the QPO is concentrated in the Peak 2/Interpulse region; P1 indicates that it is detected mainly during Peak 1. The nominal energy band in which the QPOs are seen is  $< 100$  keV except where noted. Notes: [1] Watts & Strohmayer (2006); [2] This paper; [3] Israel et al. (2005); [4] The amplitude in Watts & Strohmayer (2006) was incorrectly reported as  $10.0 \pm 0.3$  %; [5] The amplitude differs from that reported in the previous two rows because we focus on a different time period [6] Observed in the nominal 100-200 keV band

Frequency (Hz)	Width (Hz)	RMS amplitude (%)	Duration (s)	Phase	Satellite	Notes
$17.9 \pm 0.1$	$1.9 \pm 0.2$	$4.0 \pm 0.3$	60-230	P2/I	RHESSI	[1]
$25.7 \pm 0.1$	$3.0 \pm 0.2$	$5.0 \pm 0.3$	60-230	P2/I	RHESSI	[1]
$29.0 \pm 0.4$	$4.1 \pm 0.5$	$20.5 \pm 3.0$	190-260	P2/I	RXTE	[2]
$92.5 \pm 0.2$	$1.7^{+0.7}_{-0.4}$	$10.7 \pm 1.2$	150-260	P2/I	RXTE	[3]
$92.7 \pm 0.1$	$2.3 \pm 0.2$	$10.3 \pm 0.8$	150-260	P2/I	RHESSI	[1,4]
$92.9 \pm 0.2$	$2.4 \pm 0.3$	$19.2 \pm 2.0$	190-260	P2/I	RXTE	[2,5]
$150.3 \pm 1.6$	$17 \pm 5$	$6.8 \pm 1.3$	10-350	P1	RXTE	[2]
$626.46 \pm 0.02$	$0.8 \pm 0.1$	$20 \pm 3$	50-200	P1	RHESSI	[1,6]
$625.5 \pm 0.2$	$1.8 \pm 0.4$	$8.5 \pm 1.8$	190-260	P2/I	RXTE	[2]
$1837 \pm 0.8$	$4.7 \pm 1.2$	$18.0 \pm 3.6$	230-245	P2/I	RXTE	[2]